

This is the pre-peer reviewed version of the following article: Molecular dynamics study of conformational changes in human serum albumin by binding of fatty acids, *Proteins* (2006), which has been published in final form at <https://doi.org/10.1002/prot.21053>. This article may be used for non-commercial purposes in accordance with Wiley Terms and Conditions for Use of Self-Archived Versions.

Molecular dynamics study of conformational changes in human serum albumin by binding of fatty acids

Shin-ichi Fujiwara, Takashi Amisaki

Department of Biological Regulation, Faculty of Medicine, Tottori University, 86 Nishi-machi, Yonago, 683-8503, Japan

Please address correspondence to:

Shin-ichi Fujiwara, Ph.D.

Department of Biological Regulation

Faculty of Medicine

Tottori University, Yonago 683-8503, Japan

Tel: +81-859-38-6358

Fax: +81-859-38-6350

E-mail: fujiwara@grape.med.tottori-u.ac.jp

Short title: MD simulations of HSA-myristate complex

Key words: molecular dynamics simulations; human serum albumin; fatty acid; conformational changes; drug binding site; principal component analysis.

ABSTRACT

Human serum albumin (HSA) binds with fatty acids under normal physiological conditions. To date, there is little published information on the tertiary structure of HSA-fatty acid complex in aqueous solution. In the present study, we used molecular dynamics (MD) simulations to elucidate possible structural changes of HSA brought about by the binding of fatty acids. Both unliganded HSA and HSA-fatty acid complex models for MD calculations were constructed based on the X-ray crystal structures. Five myristates (MYRs) were bound in the HSA-fatty acid complex model. In the present MD study, the motion of domains I and III caused by the binding of MYR molecules increased the radius of gyration of HSA. Root mean square fluctuations from the MD simulations revealed that the atomic fluctuations of the specific amino acids at drug binding site I that can regulate the drug binding affinity were increased by the binding of MYR molecules. Primary internal motions, characterized by the first three principal components, were observed mainly at domains I and III in the principal component analysis for trajectory data. The directional motion projected on the first principal component of unliganded HSA was conserved in HSA-MYR complex as the third principal directional motion with higher frequency. On the other hand, the third principal directional motion in unliganded HSA turned into the first principal directional motion with lower frequency in HSA-MYR complex. Thus, the present MD study provides insights into the possible conformational changes of HSA caused by the binding of fatty acids.

INTRODUCTION

Human serum albumin (HSA) is a major protein component of blood plasma. HSA serves as a transport for fatty acids and for a broad spectrum of therapeutic agents, and drug binding to HSA can result in a prolonged *in vivo* half-life of the drug. Thus, the binding properties of drugs to HSA is one of the most important factors determining their pharmacokinetics.¹

HSA consists of 585 amino acids and has a molecular mass of 66500 Da. The structure of HSA consists of three homologous domains (domains I-III), each of which is divided into two subdomains, A and B, having six and four α -helices, respectively.²⁻⁴ Multiple drug binding sites have been reported for these subdomains.^{1,5,6} Among the drug binding sites, two primary binding sites, site I (the warfarin binding site, located in subdomain IIA) and site II (the indole-benzodiazepine site, located in subdomain IIIA) have received particular attention because of their high-affinity drug binding.⁵ Detailed studies have been carried out on site I, including X-ray crystallography of HSA-warfarin complex⁷ and measurements of binding affinity at site I using recombinant HSA mutants.^{8,9}

When measuring the binding affinity of a drug to HSA *in vitro*, defatted HSA is usually used. On the other hand, under normal physiological conditions, HSA binds with approximately 0.1-2 moles of fatty acid per mol protein.¹⁰ A number of studies on the effect of fatty acids on the drug binding affinity of HSA report that fatty acids may influence the drug binding affinity.¹¹⁻¹⁵ Additionally, X-ray crystal structures have been studied with respect to structural differences between unliganded HSA and HSA-myristate (HSA-MYR) complex.^{16,17} Although it is realized that solution and crystal structures of a protein are generally similar in most cases, the solution structure may not be equal to its crystal structure, which is influenced by the packing of proteins in a crystal.¹⁸ To date, little information has been published on conformational changes caused by the binding of fatty acids to HSA in aqueous solution.

X-ray crystallography and nuclear magnetic resonance (NMR) spectroscopy have been used to analyze the tertiary structures of macromolecules,^{19,20} and recently, molecular dynamics (MD)

simulations have also become a promising tool for the investigation of macromolecules. MD simulation gives insights into the natural dynamics on different timescales of macromolecules in solution, and affords thermal averages of molecular properties.^{21,22} There have been several MD simulation studies regarding HSA. MD simulations with a limited space around the N ξ atom of K199 were carried out to investigate the influence of the protonation state of K195 and K199.²³ Recently, an MD study dealing with the entire HSA molecule with explicit water molecules was also reported.²⁴ These studies provided useful information on the primary drug binding sites of HSA, however, directional motions among domains in unliganded HSA, and conformational changes brought about by the binding of fatty acids in aqueous solution have not yet been elucidated.

The present study was undertaken to elucidate the entire HSA structure in aqueous solution based on MD simulations with explicit water molecules. Our study also aimed to elucidate conformational changes as well as changes in dynamics due to the binding of fatty acids. In this paper, we present the results of 10 ns MD simulations of unliganded HSA and HSA-fatty acid complex. It was found that the atomic fluctuations of the amino acids at site I that regulate the drug binding affinity increase upon binding of MYR molecules. In addition, the present study revealed that the first principal directional motion in unliganded HSA is weakened but still present as the third principal directional motion in HSA-MYR complex. These findings may be important in understanding the effects of MYR on the drug binding affinity of HSA.

MATERIALS AND METHODS

Tertiary structure of unliganded HSA and HSA-fatty acid complex

The initial coordinates of unliganded HSA and HSA-MYR complex were obtained from the Protein Data Bank (PDB)²⁵ (unliganded HSA: PDB entry 1AO6⁴; HSA-MYR: PDB entry 1BJ5¹⁶). The resolution of the structure in each PDB entry was 2.5 Å. In PDB entry 1BJ5, five MYR molecules were bound to HSA (Fig. 1), and all were included in the following MD simulations.

MD simulations of unliganded HSA and HSA-MYR complex

A series of MD calculations (simulation and trajectory analysis) were carried out using the AMBER7 package,²⁶ using the LEaP module²⁷ for model construction of unliganded HSA and HSA-MYR complex. The Sander module was used for energy minimization and MD calculations, and the AMBER94 force field²⁸ was used for modeling the HSA system. The force field of MYR was generated by the antechamber module, based on the general AMBER force field (GAFF).²⁹ Following *ab initio* optimization of a MYR molecule at the HF/6-31G* level by Gaussian 03,³⁰ restrained electrostatic potential (RESP) was used as the charge method in GAFF.

Missing atoms were added to the initial coordinates by the LEaP module. Energy minimization with constraints on the positions of heavy atoms was carried out for 500 steps. Na⁺ counterions were placed by LEaP to neutralize the -15 (unliganded HSA) and -14 (HSA-MYR complex) charges of the HSA models at pH 7. A rectangular-shaped box of water was constructed using the TIP3 water model,³¹ with the buffering distance set to 12 Å. For the water box model, 500 steps of energy minimization constraining the HSA molecule were carried out, followed by 500 steps of energy minimization with no constraints.

After energy minimization, 10 ns MD calculations were carried out for both the unliganded HSA and HSA-MYR complex models under periodic boundary conditions. The nonbonded list was generated using an atom-based cutoff of 8 Å. The long-range electrostatic interactions were handled by the particle-mesh Ewald algorithm.³² The time step of the MD simulations was set to 2.0 fs, and the SHAKE algorithm³³ was used to constrain bond lengths at their equilibrium values. Temperature and pressure were maintained using the weak-coupling algorithm³⁴ with coupling constants τ_T and τ_P of 1.0 ps and 0.2 ps, respectively (310 K, 1 atm). Coordinates were saved for analyses every 1 ps. The resultant model systems contained 87223 (unliganded HSA) and 99126 (HSA-MYR complex) atoms.

The present MD simulations were run on an in-house PC cluster composed of 8 nodes (Pentium[®] 4 2.4 GHz, 1 GB DDR memory) with a gigabit ethernet interconnection. Trajectory analyses were carried out using the ptraj and carnal modules. Structural diagrams were prepared by

Principal component analysis for identifying global and correlated motions

Principal component analysis (PCA) is a powerful tool for finding global, correlated motions in atomic simulations of macromolecules.^{36,37} Briefly, PCA is carried out for collective coordinates from MD simulations. The collective coordinate matrix is a $3N \times T$ matrix, where N is the number of atoms considered, and T is the number of the coordinate set collected by the simulations. The collected coordinate matrix can be used to construct a covariance matrix A , whose (i, j) component is defined as:

$$A_{ij} = \langle (x_i - \langle x_i \rangle)(x_j - \langle x_j \rangle) \rangle \quad (1)$$

where $\langle \dots \rangle$ is the average over the T sampled data and x_i is a mass-weighted atomic coordinate. The diagonalization of A yields the eigenvectors and eigenvalues, which represent the components and magnitudes of atomic fluctuations, respectively. In a protein, a few modes contain more than half of the total fluctuation in the system, and the first few modes usually describe global, collective motions. To verify the relevance of the eigenvectors, the overlap³⁸ between two sets of n orthonormal eigenvectors $\{\mathbf{v}_1, \dots, \mathbf{v}_n\}$ and $\{\mathbf{w}_1, \dots, \mathbf{w}_n\}$, was calculated as follows:

$$overlap(\mathbf{v}, \mathbf{w}) = \frac{1}{n} \sum_{i=1}^n \sum_{j=1}^n (\mathbf{v}_i \cdot \mathbf{w}_j)^2 \quad (2)$$

To estimate how much of the major essential modes from the covariance analysis resemble random diffusion, its cosine content³⁹ c_i of the eigenvector i was calculated as follows:

$$c_i = \frac{2}{T} \left(\int_0^T \cos(i\pi t) p_i(t) dt \right)^2 \left(\int_0^T p_i^2(t) dt \right)^{-1} \quad (3)$$

where $p_i(t)$ is the amplitude of the motion along eigenvector i at time t . The cosine content can take values between 0 (no cosine) and 1 (a perfect cosine), and provides an indicator of the extent of sampling.

A series of PCA calculations was carried out on the trajectory data of both unliganded HSA and HSA-MYR complex systems using the quasih module⁴⁰ of the AMBER7 package. Directional

motion projected on each eigenvector was visualized by the interactive essential dynamics plug-in⁴¹ in VMD.

Entropy calculation from covariance matrices of the atomic fluctuations

The change in configurational entropy of HSA molecule by the binding of MYR was estimated from the results of the PCA for the mass-weighted covariance matrix A . The configurational entropy was calculated as follows⁴²:

$$S = k_B \sum_i^{3N-6} \left\{ \frac{h\omega_i/k_B T}{e^{h\omega_i/k_B T} - 1} - \ln(1 - e^{-h\omega_i/k_B T}) \right\} \quad (4)$$

where k_B , h , T , ω_i are the Boltzmann constant, the Planck constant, the absolute temperature, and the quasiharmonic frequency ($=\sqrt{k_B T/\lambda_i}$, λ_i : eigenvalue) for the i -th eigenvector, respectively. To estimate contributions to the change in the configurational entropy upon binding, the contribution ratio of the entropic cost in the binding free energy ($=\Delta H - T\Delta S$) was calculated as follows:

$$\text{contribution ratio} = \frac{\|T\Delta S\|}{\|\Delta H\| + \|T\Delta S\|} \quad (5)$$

where ΔS and ΔH are the changes in the configurational entropy and the enthalpy of both HSA and MYR molecules, respectively.

RESULTS AND DISCUSSION

Root mean square deviation of unliganded HSA and HSA-MYR complex systems

The root mean square deviation (RMSD) from the X-ray structure provides a direct measure of the structural drift from the initial coordinates as well as the atomic fluctuation over the course of an MD simulation. The RMSD values of heavy atoms in unliganded HSA and HSA-MYR complex systems are shown in Fig. 2. In both systems, RMSD values reached plateau at about 2 ns (Fig. 2A). Calculated from the 2.5-10 ns trajectory data, the RMSD values of heavy atoms in the whole HSA molecule were 3.69 ± 0.35 Å and 3.42 ± 0.38 Å for unliganded HSA and HSA-MYR complex, respectively. Hence, we conclude that no significant structural drift from the X-ray structure occurred

during the MD simulations.

With respect to the RMSD of heavy atoms at drug binding site I (Fig. 2B), the RMSD values were 2.20 ± 0.12 Å for unliganded HSA and 2.23 ± 0.31 Å for HSA-MYR complex, calculated from the 2.5-10 ns trajectory data. These RMSD values were smaller than those of the whole HSA molecule, indicating that site I exhibited smaller atomic fluctuation; that is, site I is a relatively rigid region in the whole HSA molecule. The RMSD values of the other primary drug binding site, site II, were also small (2.19 ± 0.15 Å for unliganded HSA and 1.81 ± 0.13 Å for HSA-MYR complex, calculated from the 2.5-10 ns trajectory data). Thus, it was suggested that both primary drug binding sites I and II are relatively rigid.

Radius of gyration of unliganded HSA and HSA-MYR complex systems

In the present MD studies, we determined the radius of gyration (Rg) as shown in Fig. 3. In both systems, Rg values reached plateau at about 2 ns, indicating that the MD simulations achieved equilibrium after 2 ns. The Rg value of HSA experimentally measured in aqueous solution is reported to be 27.4 ± 0.35 Å.⁴³ In the present study, the Rg value of the unliganded HSA model was 27.20 ± 0.23 Å, calculated from the 2.5-10 ns trajectory data. This coincidence indicates that the equilibrium state of HSA molecule in aqueous solution was well reproduced in the present MD studies.

The binding of MYR to HSA was found to increase the Rg of unliganded HSA in the present MD simulations (Fig. 3). Calculated from the 2.5-10 ns trajectory data, the Rg value of HSA-MYR complex was 28.28 ± 0.22 Å, larger than that of unliganded HSA. To clarify the origin of this increase in Rg upon binding to MYR, we conducted a comparison of the average structures of unliganded HSA and HSA-MYR complex using the 2.5 to 10 ns MD trajectory. Table I shows the RMSD in C α atom positions after the superposition of the two averaged structures using residues in domain II or in individual domains. At domain II, little change was observed in the conformation of HSA by the binding of MYR molecules. On the other hand, a dramatic increase was observed in the relative motions of domains I and III, especially those of subdomains IA, IB, and IIIB. These observations are

consistent with those reported by Curry et al. in their X-ray crystal study.¹⁶ Thus, we expected to see the increase observed in R_g due to the binding of MYR molecules for HSA in aqueous solution (Fig. 3) as well as in its crystalline state, and this increase was caused by the motions of domains I and III.

Equilibrium fluctuations of unliganded HSA and HSA-MYR complex systems

Local protein mobility was analyzed by calculating the time-averaged root mean square fluctuation (RMSF) for each residue, based on the 2.5-10 ns trajectory data (Fig. 4). For comparison with experimental data, the B-factors of the X-ray crystal structure were converted to the equivalent RMSF values. The RMSF values of unliganded HSA (Fig. 4A) and HSA-MYR complex (Fig. 4B) were plotted against residue numbers. The general profiles of atomic fluctuations were found to be very similar to each other. It is worthwhile to note that, at drug binding sites I (subdomain IIA, residues 197-297) and II (subdomain IIIA, residues 384-497), the RMSF values in the MD studies were small compared with those of other regions (Fig. 4, Table II). Such profiles, i.e., smaller RMSF values at sites I and II, can be seen in both unliganded HSA (Fig. 4A) and HSA-MYR complex models (Fig. 4B). These results suggest that the structure of primary drug binding sites I and II remains rigid. However, this profile was not observed in the experimental RMSF values derived from B-factors. Considering the relatively low resolution of the X-ray structures (2.5 Å), it is likely that the B-factors in this case do not accurately reflect the thermal fluctuations of atoms. Thus, the present MD studies revealed the smaller atomic fluctuations at sites I and II, which may be characteristic of HSA molecule.

To investigate in detail the profile of the atomic fluctuation at drug binding site I, the RMSF value of each amino acid residue at the site was determined (Fig. 5). Here, we focused on mutated residues of HSA mutants belonging to site I, which have been reported to alter the binding affinity of site I drugs.^{8,9,44,45} Of these amino acid residues, K195, K199, R218, R222, H242 and H257 are positively charged residues which surround the entrance of the binding pocket of site I,⁴ while F211 and W214 form the benzyl moiety in the binding pocket.⁷ In the present MD study, many of the

residues showed smaller RMSF values, suggesting that amino acids that can affect binding affinity in HSA molecules have very small atomic fluctuations; in other words, these amino acid residues are rigid as compared with other residues.

The effect of MYR binding to HSA on atomic fluctuations is shown in Table II. RMSF values at drug binding sites I (subdomain IIA) and II (subdomain IIIA) were not so much different. However, RMSF values of the specific amino acid residues were increased by the binding of MYR (Fig. 5), suggesting that the binding affinity of site I drugs can be changed by MYR binding. As reported previously,^{11,12,14,15} fatty acids at high concentrations regulate the drug binding affinity of HSA in a complex manner. Thus, we suggest that the changes in atomic fluctuation observed in the present MD study influence the binding affinity of drugs.

Principal component analysis for analyzing correlated motions of unliganded HSA and HSA-MYR complex

In order to analyze the internal motions of the whole HSA molecule as well as those of each domain, PCA was carried out using the 2.5-10 ns trajectory data of C α atoms. In the present analysis, all structures were least squares fitted on the position of C α atoms at time 2.5 ns to remove overall translation and rotation. Fig. 6 shows the RMS fluctuations along the first 50 eigendirections (square roots of eigenvalues divided by mass-weight) of the covariance matrix derived from the unliganded and liganded HSA trajectory. Compared with the whole HSA molecule (Fig. 6A), RMS fluctuations along the eigendirections of the covariance matrix derived from the trajectory of drug binding site I were much smaller than those from the whole HSA (Fig. 6B), indicating that the internal motions at site I are much smaller than those of the whole HSA molecule.

To verify the relevance of the eigenvectors derived from the unliganded HSA and HSA-MYR complex models, we calculated the overlap between the subspaces spanned by the eigenvectors. The first 10 eigenvectors were adopted for analysis as representing the primary internal motions of the whole HSA molecule, whose contribution ratios were 79.8% and 82.6% for unliganded HSA and

HSA-MYR complex, respectively. Table III shows the overlap of the first 10 principal components between the subspaces of unliganded HSA and HSA-MYR complex spanned by the eigenvectors. The overlap value observed at the whole molecule between unliganded HSA and HSA-MYR complex was 0.476 for the first 10 principal components. In addition, the smaller the spatial region (the number of C α atoms), the larger the overlap between unliganded HSA and HSA-MYR complex. This result indicates that, as a result of the binding of MYR to unliganded HSA, the interdomain motions were changed more than intradomain motions.

To analyze the primary internal motions in the whole HSA molecule in detail, we focused on the first three principal components (PCs), whose contribution ratios were much larger than those of the other PCs (41.3%, 14.2%, and 9.9% for the unliganded HSA model, respectively, and 47.2%, 10.8%, 7.2% for the HSA-MYR complex model). Fig. 7 shows the fluctuations of C α atoms projected on the first three principal components, PC1, PC2, and PC3. In both the unliganded HSA and HSA-MYR complex systems, fluctuations were smaller at domain II (residues 197-383), but larger at domain I (residues 5-196) and domain III (residues 384-582). Thus, the primary internal motions can be seen primarily at domains I and III.

We used the interactive essential dynamics plug-in⁴¹ to visualize the directions of motion projected on the principal components, PC1, PC2, and PC3 (Fig. 8). In both unliganded HSA and HSA-MYR complex systems, cooperative motions between domains I and III were observed on the three principal components. To check the similarity of the direction of motion, the inner product between each principal component was calculated (Table IV). The direction of motion projected on PC1 of unliganded HSA (PC1_{HSA}) was very similar to that projected on PC3 of HSA-MYR complex (PC3_{HSA-MYR}). The inner product between PC1_{HSA} and PC3_{HSA-MYR} showed a high absolute value of -0.635, indicating that vectors PC1_{HSA} and PC3_{HSA-MYR} are similar in direction. In addition, the inner product between PC3_{HSA} and PC1_{HSA-MYR} also showed a high absolute value of 0.592. On the other hand, the quasiharmonic frequency of the cooperative motion for each principal component,

calculated as $\sqrt{k_B T / \lambda_i}$, was not so much changed by the binding of MYR (Table IV). These results suggest that the $PC1_{\text{HSA}}$ directional motion observed in unliganded HSA was conserved in HSA-MYR complex as the $PC3_{\text{HSA-MYR}}$ directional motion with higher frequency, and that, on the other hand, the $PC3_{\text{HSA}}$ directional motion in unliganded HSA turned into the $PC1_{\text{HSA-MYR}}$ directional motion with lower frequency in HSA-MYR complex. Thus, the present MD study successfully elucidated differences in the first three principal directional motions between unliganded HSA and HSA-MYR complex.

Regarding PCA, Hess^{38,39} pointed out that the sampling is far from converged when the first few principal components resemble cosines. We calculated the cosine contents of the first three principal components obtained from the 2.5-10 ns trajectory data using Eq. 3. The cosine contents, c_1 , c_2 , and c_3 were 0.744, 0.072, 0.060 for unliganded HSA, and 0.530, 0.544, 0.009 for HSA-MYR complex. The cosine contents of the PC1 showed relatively high values, implying that the fluctuations of PC1 might be caused by random diffusion because of the insufficient sampling. However, as described previously, the directional motions of the first principal component ($PC1_{\text{HSA}}$, $PC1_{\text{HSA-MYR}}$) in HSA molecule were also observed as the directional motions of the third principal component ($PC3_{\text{HSA-MYR}}$, $PC3_{\text{HSA}}$), whose fluctuations are not likely to be caused by random diffusion from the view of the cosine content, c_3 . Therefore, we believe that PC1 directional motions ($PC1_{\text{HSA}}$, $PC1_{\text{HSA-MYR}}$) do not arise from a random diffusion. In addition, by increasing the sampling period, more conformational freedom could be extracted. Table V shows the subspace overlap of the first three principal components between the sections of the 2.5-10 ns trajectory. The overlap between the 2.5-ns subsets (2.5-5.0, 5.0-7.5, 7.5-10 ns) was low, but was relatively high between the 7.5-ns subset (2.5-10 ns) and each 2.5-ns subset. Although the way to get a full impression of the conformational freedom of HSA is to perform a longer MD simulation, a length more than 10 ns simulation for HSA is currently beyond our computational resources.

Change in configurational entropy of unliganded HSA by binding of fatty acid

Ligand binding is often associated with losses in configurational entropy.⁴⁶ In the present study, we estimated the change in configurational entropy by the binding of MYR to HSA from the principal component analysis. Table VI shows the configurational entropy calculated from Eq. 4. The configurational entropy of unliganded HSA became small by the binding of five MYR molecules. The magnitude of the entropic cost of HSA molecule, $\|T\Delta S_{HSA}\|$, was 7.6 kcal/mol (310 K), calculated from the result of the 2.5-10 ns trajectory, and the magnitude of the entropic cost of both HSA and five MYR molecules ($\|T\Delta S\| = \|T\Delta S_{HSA} + T\Delta S_{5MYR}\|$) was considered to be > 7.6 kcal/mol in the binding free energy. On the other hand, for the binding of one MYR molecule, the magnitude was reported to be 0.57 kcal/mol (298 K).⁴⁷ Assuming that the magnitude of the enthalpic cost of one MYR binding is the same ($= \|\Delta H\|$) at each MYR binding site, the contribution ratios of the entropic cost in the binding free energy were calculated from Eq. 5 as $0.57/(\|\Delta H\| + 0.57)$ and $> 7.6/(5\|\Delta H\| + 7.6)$ for one MYR molecule and five MYR molecules, respectively. Although each sampling was not fully converged as described previously, the results suggest that increasing the number of MYR binding to HSA causes the increase in the ratio of entropic cost in the binding free energy. In fact, HSA binds with approximately 0.1-2 moles of fatty acid per mol protein under normal physiological condition.¹⁰ In the point of the contribution ratio of the enthalpic and the entropic cost in the binding free energy, less than two fatty acid molecules may be favorable for the binding to HSA.

CONCLUSION

In the present study, the effect of the binding of fatty acids on the tertiary structure of HSA in aqueous solution was discussed based on the results of MD simulations. The primary HSA drug binding sites, I and II, showed relatively small RMSF values on average. The flexibility of the specific amino acids at site I that can regulate the drug binding affinity was increased by the binding of MYR molecules. In PCA, primary internal motions, characterized by the first three principal components, were observed primarily at domains I and III. The first principal directional motion in

unliganded HSA was conserved in HSA-MYR complex as the third principal directional motion with higher frequency, while the third principal directional motion in unliganded HSA turned into the first principal directional motion with lower frequency in HSA-MYR complex. Thus, the present study unraveled possible conformational changes caused by the binding of MYR molecules to HSA. To estimate more strictly the tertiary structure of HSA under normal physiological conditions by MD simulations, however, more physiological information is required, such as the relative affinity of fatty acid binding sites, and the kind of fatty acids bound to HSA. Simulations over longer time periods are also preferable for further detail investigation of the effect of fatty acid binding. Nevertheless, the present MD study successfully provided insights on the tertiary structure of HSA-fatty acid complex in aqueous solution as a step toward elucidating HSA under normal physiological conditions. Specifically, the present study makes an important contribution to understanding the effect of the binding of fatty acids on conformational changes of HSA in aqueous solution.

ACKNOWLEDGEMENTS

This study was supported in part by Grants-in-Aid for Scientific Research from the Ministry of Education, Culture, Sports, Science and Technology of Japan.

References

1. Kragh-Hansen U, Chuang VTG, Otagiri M. Practical aspects of the ligand-binding and enzymatic properties of human serum albumin. *Biol Pharm Bull* 2002;25:695–704.
2. He XM, Carter DC. Atomic structure and chemistry of human serum albumin. *Nature* 1992;358:209–215.
3. Dockal M, Carter DC, Ruker F. The three recombinant domains of human serum albumin. Structural characterization and ligand binding properties. *J Biol Chem* 1999;274:29303–29310.
4. Sugio S, Kashima A, Mochizuki S, Noda M, Kobayashi K. Crystal structure of human serum albumin at 2.5 Å resolution. *Prot Eng* 1999;12:439–446.
5. Sudlow G, Birkett DJ, Wade DN. The characterization of two specific drug binding sites on human serum albumin. *Mol Pharmacol* 1975;21:824–832.
6. Sjöholm I, Ekman B, Kober A, Ljungstedt-Pahlman I, Seiving B, Sjödin T. Binding of drugs to human serum albumin: XI. The specificity of three binding sites as studied with albumin immobilized in microparticles. *Mol Pharmacol* 1979;16:767–777.
7. Petitpas I, Bhattacharya AA, Twine S, East M, Curry S. Crystal structure analysis of warfarin binding to human serum albumin: anatomy of drug site I. *J Biol Chem* 2001;276:22804–22809.
8. Petersen CE, Ha CE, Curry S, Bhagavan NV. Probing the structure of the warfarin-binding site on human serum albumin using site-directed mutagenesis. *Proteins* 2002;47:116–125.
9. Watanabe H, Kragh-Hansen U, Tanase S, Nakajou K, Mitarai M, Iwao Y, Maruyama T, Otagiri M. Conformational stability and warfarin-binding properties of human serum albumin studied by recombinant mutants. *Biochem J* 2001;357:269–274.
10. Fredrickson DS, Gordon RS. The metabolism of albumin-bound C¹⁴-labeled unesterified fatty acids in normal human subjects. *J Clin Invest* 1958;37:1504–1515.
11. Dasgupta A, Crossey MJ. Elevated free fatty acid concentrations in lipemic sera reduce protein binding of valproic acid significantly more than phenytoin. *Am J Med Sci* 1997;313:75–79.
12. Takamura N, Shinozawa S, Maruyama T, Suenaga A, Otagiri M. Effects of fatty acids on serum

- binding between furosemide and valproic acid. *Biol Pharm Bull* 1998;21:174–176.
13. Petitpas I, Grune T, Bhattacharya AA, Curry S. Crystal structures of human serum albumin complexed with monounsaturated and polyunsaturated fatty acids. *J Mol Biol* 2001;314:955–960.
 14. Chuang VT, Otagiri M. How do fatty acids cause allosteric binding of drugs to human serum albumin? *Pharm Res* 2002;19:1458–1464.
 15. Vorum H, Honoré B. Influence of fatty acids on the binding of warfarin and phenprocoumon to human serum albumin with relation to anticoagulant therapy. *J Pharm Pharmacol* 1996;48:870–875.
 16. Curry S, Mandelkow H, Brick P, Franks N. Crystal structure of human serum albumin complexed with fatty acid reveals an asymmetric distribution of binding sites. *Nat Struct Biol* 1998;5:827–835.
 17. Curry S, Brick P, Franks N. Fatty acid binding to human serum albumin: new insights from crystallographic studies. *Biochim Biophys Acta* 1999;1441:131–140.
 18. Garbuzynskiy SO, Melnik BS, Lobanov MY, Finkelstein AV, Galzitskaya OV. Comparison of X-ray and NMR structures: is there a systematic difference in residue contacts between X-ray- and NMR-resolved protein structures? *Proteins* 2005;60:139–147.
 19. Brünger AT. X-ray crystallography and NMR reveal complementary views of structure and dynamics. *Nat Struct Biol* 1997;4:862–865.
 20. Russell RB, Alber F, Aloy P, Davis FP, Korkin D, Pichaud M, Topf M, Sali A. A structural perspective on protein-protein interactions. *Curr Opin Struct Biol* 2004;14:313–324.
 21. Feig M, Brooks CL 3rd. Recent advances in the development and application of implicit solvent models in biomolecule simulations. *Curr Opin Struct Biol* 2004;14:217–224.
 22. Norberg J, Nilsson L. Advances in biomolecular simulations: methodology and recent applications. *Q Rev Biophys* 2003;36:257–306.
 23. Díaz N, Suárez D, Sordo TL, Merz KM Jr. Molecular dynamics study of the IIA binding site in human serum albumin: influence of the protonation state of Lys195 and Lys199. *J Med Chem*

2001;44:250–260.

24. Artali R, Bombieri G, Calabi L, Del Pra A. A molecular dynamics study of human serum albumin binding sites. *Farmaco* 2005;60:485–495.
25. Berman HM, Westbrook J, Feng Z, Gilliland G, Bhat TN, Weissig H, Shindyalov IN, Bourne PE. The Protein Data Bank. *Nucleic Acids Res* 2000;28:235–242.
26. Case DA, Pearlman DA, Caldwell JW, Cheatham TE 3rd, Wang J, Ross WS, Simmerling CL, Darden TA, Merz KM, Stanton RV, Cheng AL, Vincent JJ, Crowley M, Tsui V, Gohlke H, Radmer RJ, Duan Y, Petera J, Massova I, Seibel GL, Singh UC, Weiner PK, Kollman PA. *AMBER7*. San Francisco: University of California; 2002.
27. Schafmeister C, Ross WS, Romanovski V. *LEAP*. San Francisco: University of California; 1997.
28. Cornell WD, Cieplak P, Bayly CI, Gould IR, Merz KM Jr, Ferguson DM, Spellmeyer DC, Fox T, Caldwell JW, Kollman PA. A second generation force field for the simulation of proteins, nucleic acids, and organic molecules. *J Am Chem Soc* 1995;117:5179–5197.
29. Wang J, Wolf RM, Caldwell JW, Kollman PA, Case DA. Development and testing of a general Amber force field. *J Comp Chem* 2004;25:1157–1173.
30. Frisch MJ, Trucks GW, Schlegel HB, Scuseria GE, Robb MA, Cheeseman JR, Montgomery JA Jr, Vreven T, Kudin KN, Burant JC, Millam JC, Iyengar SS, Tomasi J, Barone V, Mennucci B, Cossi M, Scalmani G, Rega N, Petersson GA, Nakatsuji H, Hada M, Ehara M, Toyota K, Fukuda R, Hasegawa J, Ishida M, Nakajima T, Honda Y, Kitao O, Nakai H, Klene M, Li X, Knox JE, Hratchian HP, Cross JB, Adamo C, Jaramillo J, Gomperts R, Stratmann RE, Yazyev O, Austin AJ, Cammi R, Pomelli C, Ochterski JW, Ayala PY, Morokuma K, Voth GA, Salvador P, Dannenberg JJ, Zakrzewski VG, Dapprich S, Daniels AD, Strain MC, Farkas O, Malick DK, Rabuck AD, Raghavachari K, Foresman JB, Ortiz JV, Cui Q, Baboul AG, Clifford S, Cioslowski J, Stefanov BB, Liu G, Liashenko A, Piskorz P, Komaromi I, Martin RL, Fox DJ, Keith T, Al-Laham MA, Peng CY, Nanayakkara A, Challacombe M, Gill PMW, Johnson B, Chen W, Wong MW, Gonzalez C, Pople JA. *Gaussian 03, Revision A.1*. Pittsburgh: Gaussian Inc.; 2003.

31. Jorgensen WL, Chandrasekhar J, Madura JD, Impey RW, Klein ML. Comparison of simple potential functions for simulating liquid water. *J Chem Phys* 1983;79:926–935.
32. Darden T, York D, Pedersen L. Particle mesh Ewald – an $N\log(N)$ method for Ewald sums in large systems. *J Chem Phys* 1993;98:10089–10092.
33. Van Gunsteren WF, Berendsen HJC. Algorithm for macromolecular dynamics and constraint dynamics. *Mol Phys* 1977;34:1311–1327.
34. Berendsen HJC, Postma JPM, van Gunsteren WF, DiNola A, Haak JR. Molecular dynamics with coupling to an external bath. *J Chem Phys* 1984;81:3684–3690.
35. Humphrey W, Dalke A, Schulten K. VMD – Visual Molecular Dynamics. *J Mol Graph* 1996;14:33–38.
36. Levy RM, Srinivasan AR, Olson WK, McCammon JA. Quasi-harmonic method for studying very low frequency modes in proteins. *Biopolymers* 1984;23:1099–1112.
37. Kitao A, Go N. Investigating protein dynamics in collective coordinate space. *Curr Opin Struct Biol* 1999;9:164–169.
38. Hess B. Similarities between principal components of protein dynamics and random diffusion. *Phys Rev E* 2000;62:8438–8448.
39. Hess B. Convergence of sampling in protein simulations. *Phys Rev E* 2002;65:031910.
40. Levy RM, Karplus M, Kushick J, Perahia D. Evaluation of the configurational entropy for proteins: application to molecular dynamics simulations of an α -helix. *Macromolecules* 1984;17:1370–1374.
41. Mongan J. Interactive essential dynamics. *J Comput Aided Mol Des* 2004;18:433–436.
42. Andricioaei I, Karplus M. On the calculation of entropy from covariance matrices of the atomic fluctuations. *J Chem Phys* 2001;115:6289–6292.
43. Kiselev MA, Gryzunov YA, Dobretsov GE, Komarova MN. Size of a human serum albumin molecule in solution. *Biofizika* 2001;46:423–427.
44. Petersen CE, Ha CE, Harohalli K, Park DS, Bhagavan NV. Familial dysalbuminemic

- hyperthyroxinemia may result in altered warfarin pharmacokinetics. *Chem Bio Interact* 2000;124:161–172.
45. Petitpas I, Petersen CE, Ha CE, Bhattacharya AA, Zunszain PA, Ghuman J, Bhagavan NV, Curry S. Structural basis of albumin-thyroxine interactions and familial dysalbuminemic hyperthyroxinemia. *Proc Natl Acad Sci USA* 2003;100:6440–6445.
46. Cooper A. Thermodynamic analysis of biomolecular interactions. *Curr Opin Chem Biol* 1999;3:557–563.
47. Pedersen AO, Honoré B, Brodersen R. Thermodynamic parameters for binding of fatty acids to human serum albumin. *Eur J Biochem* 1990;190:497–502.

Table I. Comparison of the average structures of unliganded human serum albumin (HSA) and HSA-myristate (HSA-MYR) complex in the MD simulations.^a

Domain	RMSD (Å)		Subdomain	RMSD (Å)	
	Overall ^b	By domain ^c		Overall ^b	By subdomain ^c
I [5-196]	10.8 (8.8)	2.4 (1.3)	IA [5-107]	13.9 (10.7)	2.0 (1.3)
			IB [108-196]	5.0 (5.9)	1.5 (1.0)
II [197-383]	1.4 (0.8)	1.4 (0.8)	IIA [197-297]	1.2 (0.9)	1.0 (0.8)
			IIB [298-383]	1.5 (0.7)	1.3 (0.6)
III [384-582]	4.1 (6.8)	1.9 (1.4)	IIIA [384-497]	2.3 (3.3)	1.1 (1.0)
			IIIB [498-582]	5.7 (9.6)	1.9 (1.4)

^aNumbers in round brackets are root mean square deviations (RMSDs) at the X-ray crystal structure between PDB entries 1AO6 and 1BJ5, as previously reported by Curry et al.¹⁶

^bRMSD in C α atom positions between domains after the superposition of the two molecules using the residues in domain II.

^cRMSD in C α atom positions after superposing the individual domains from the unliganded HSA and HSA-MYR complex structures.

Table II. Root mean square fluctuation of C α atoms (\AA) for the whole HSA molecule, and for subdomains IIA and IIIA.

	Whole molecule	Subdomain IIA	Subdomain IIIA
Unliganded HSA	1.53	1.05	1.30
HSA-MYR complex	1.65	1.07	1.36

Table III. Overlap of the first 10 principal components between the subspaces of unliganded HSA and HSA-MYR complex spanned by the eigenvectors.

	No. Atoms^a	Overlap^b
Whole molecule	578	0.476
Domain I	192	0.542
II	187	0.550
III	199	0.565
Subdomain IA	103	0.506
IB	89	0.643
IIA	101	0.630
IIB	86	0.647
IIIA	114	0.595
IIIB	84	0.651

^aNumber of C α atoms used for the principal component analysis.

^bOverlap between the subspaces spanned by the eigenvectors, as calculated by Eq. 2.

Table IV. Inner product between the first three principal components of unliganded HSA and HSA-MYR complex.^a

	PC1 _{HSA-MYR} (5.29 cm ⁻¹)	PC2 _{HSA-MYR} (11.04 cm ⁻¹)	PC3 _{HSA-MYR} (13.55 cm ⁻¹)
PC1 _{HSA} (5.81 cm ⁻¹)	0.296	-0.368	-0.635
PC2 _{HSA} (9.92 cm ⁻¹)	0.011	0.332	0.100
PC3 _{HSA} (11.84 cm ⁻¹)	0.592	0.259	-0.072

^aNumbers in round brackets are the quasiharmonic frequency, calculated as $\sqrt{k_B T / \lambda_i}$, where λ_i , k_B , T are the eigenvalue for the principal component i , the Boltzmann constant, and the absolute temperature, respectively.

Table V. Overlap of the first three principal components between the sections of the 2.5-10 ns trajectory.^a

Unliganded HSA	2.5-5.0 ns	5.0-7.5 ns	7.5-10 ns	2.5-10 ns
2.5-5.0 ns	1	0.457	0.361	0.547
5.0-7.5 ns		1	0.408	0.603
7.5-10 ns			1	0.590
2.5-10 ns				1
HSA-MYR complex	2.5-5.0 ns	5.0-7.5 ns	7.5-10 ns	2.5-10 ns
2.5-5.0 ns	1	0.471	0.589	0.697
5.0-7.5 ns		1	0.555	0.572
7.5-10 ns			1	0.810
2.5-10 ns				1

^aOverlap is calculated by Eq. 2.

Table VI. Configurational entropy of unliganded HSA and HSA-MYR complex estimated from the result of the principal component analysis.^a

Sampling	S_{HSA}	$S_{\text{HSA-MYR}}$	ΔS_{HSA}
2.5-5.0 ns	0.711	0.707	-0.004
2.5-7.5 ns	0.776	0.760	-0.016
2.5-10 ns	0.818	0.793	-0.025

^aConfigurational entropy (S) is calculated by Eq. 4. All entropies are in kcal/mol · K.

Figure Legends

Fig. 1. Ribbon model of human serum albumin-myristate (HSA-MYR) complex derived from X-ray crystallography (PDB entry 1BJ5¹⁶). HSA is composed of three homologous domains I-III. Each domain is divided into two subdomains, A and B. The five MYR molecules are shown in black in a space-filling representation. This diagram was generated using VMD.³⁵

Fig. 2. Time evolution of the root mean square deviation (RMSD) of heavy atoms from the starting structure during 10 ns molecular dynamics (MD) simulations of unliganded HSA and HSA-MYR complex models. RMSD values reached plateau at about 2 ns. **A:** all heavy atoms; **B:** heavy atoms belonging to drug binding site I (subdomain IIA).

Fig. 3. Time evolution of the radius of gyration (Rg) during 10 ns MD simulations of unliganded HSA and HSA-MYR complex. Rg values reached plateau at about 2 ns.

Fig. 4. Comparison of the root mean square fluctuation (RMSF) of C α atoms along the sequence derived from the 2.5-10 ns MD simulations (solid line) and X-ray crystal structure (thin line). RMSF values derived from the X-ray crystal structure were calculated as $\sqrt{3B/(8\pi^2)}$, where B is the temperature factor (B-factor) listed in the PDB files. At drug binding sites I and II, the RMSF values in the present MD studies were small compared with those of other regions. **A:** unliganded HSA; **B:** HSA-MYR complex.

Fig. 5. Root mean square fluctuation (RMSF) of C α atoms at drug binding site I. The amino acids whose mutations affected binding affinity at drug binding site I are also shown. Many of these amino acids showed smaller fluctuations.

Fig. 6. Root mean square fluctuation along the eigendirections (square-roots of eigenvalues divided by mass-weight) of the coordinate covariance matrix constructed from C α atoms of unliganded HSA and HSA-MYR complex. The fluctuations of drug binding site I were much smaller than those of the whole HSA molecule. **A:** all C α atoms; **B:** C α atoms belonging to drug binding site I.

Fig. 7. Root mean square fluctuation of C α atoms on the first, second, and third principal

components (PC1, PC2, PC3). The contribution ratio of each principal component is shown in round brackets. The atomic fluctuation is larger primarily at domains I and III.

Fig. 8. Directional motions projected on the first, second, and third principal components. The arrows in the figure indicate the approximate directions of cooperative motions observed by interactive essential dynamics. The directional motion projected on PC1 of unliganded HSA was similar to that projected on PC3 of HSA-MYR complex (the inner product between $PC1_{HSA}$ and $PC3_{HSA-MYR}$ was equal to -0.635).

Fig. 1

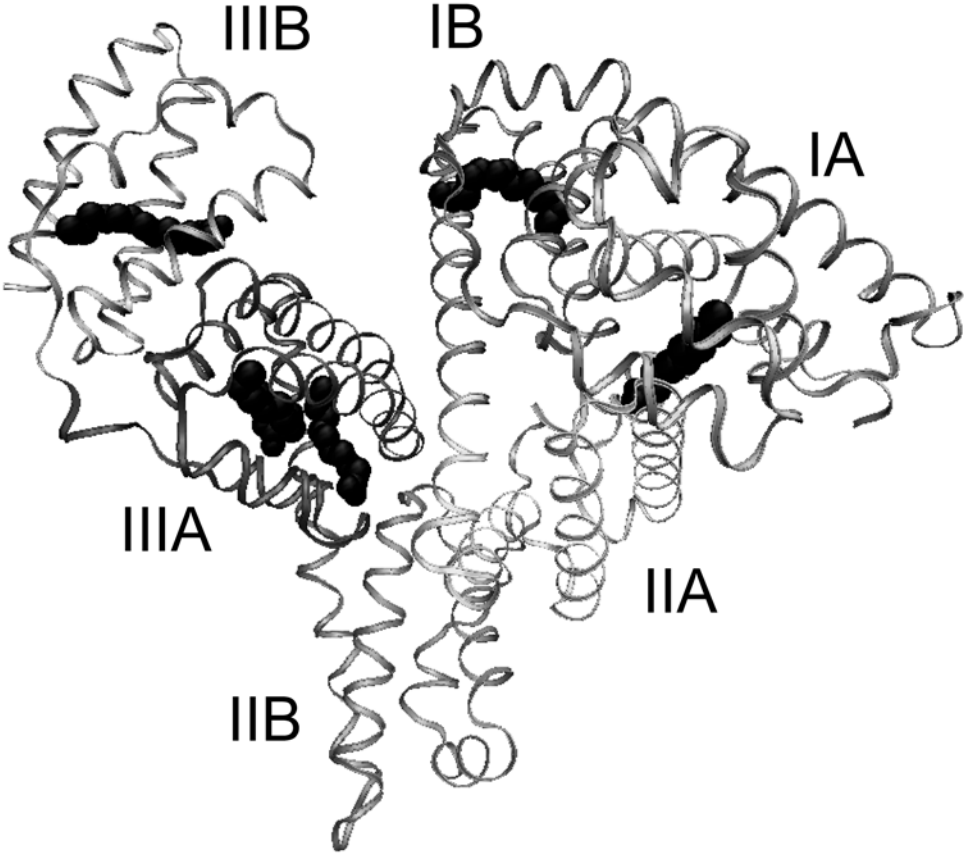


Fig. 2

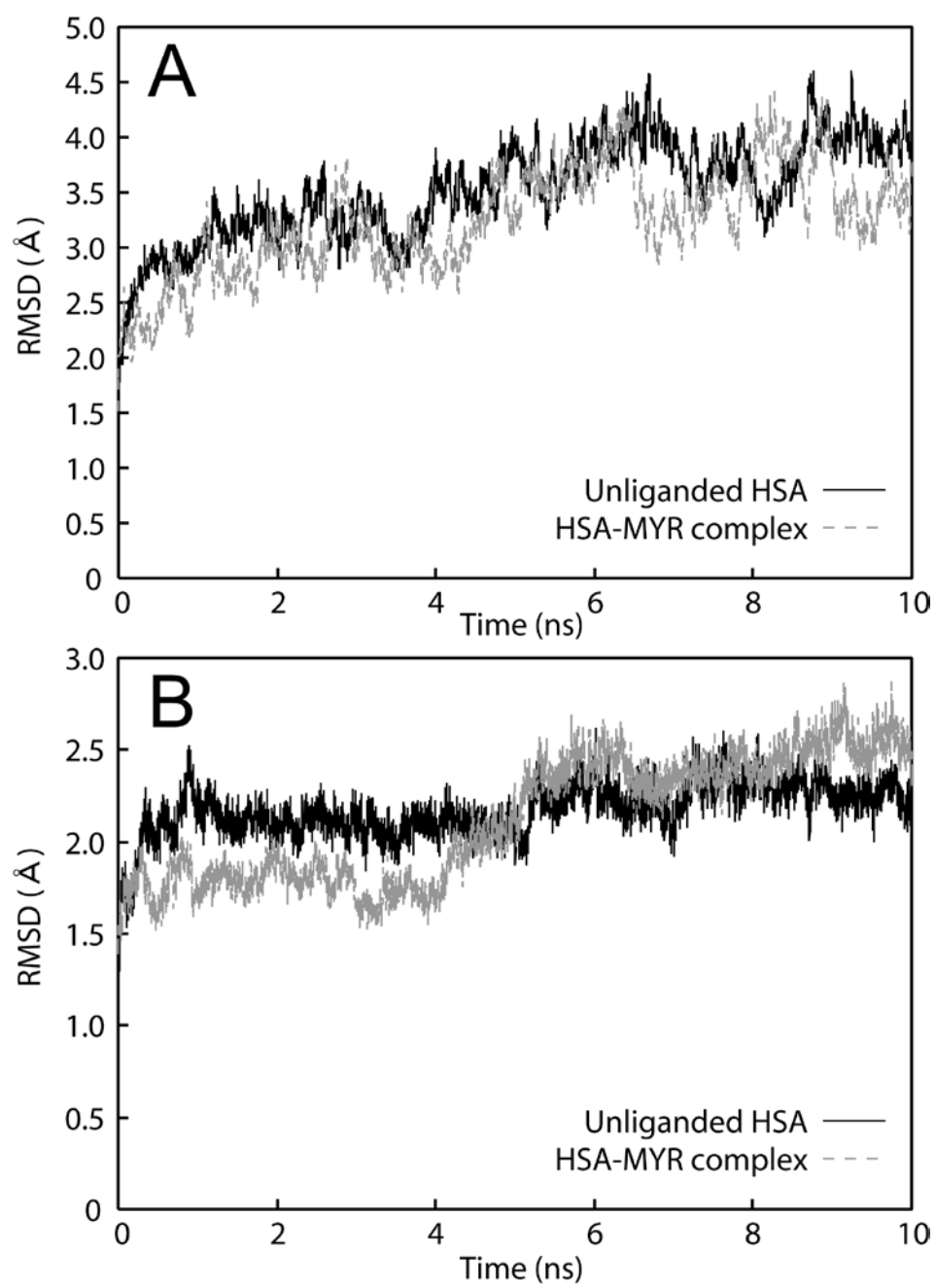


Fig. 3

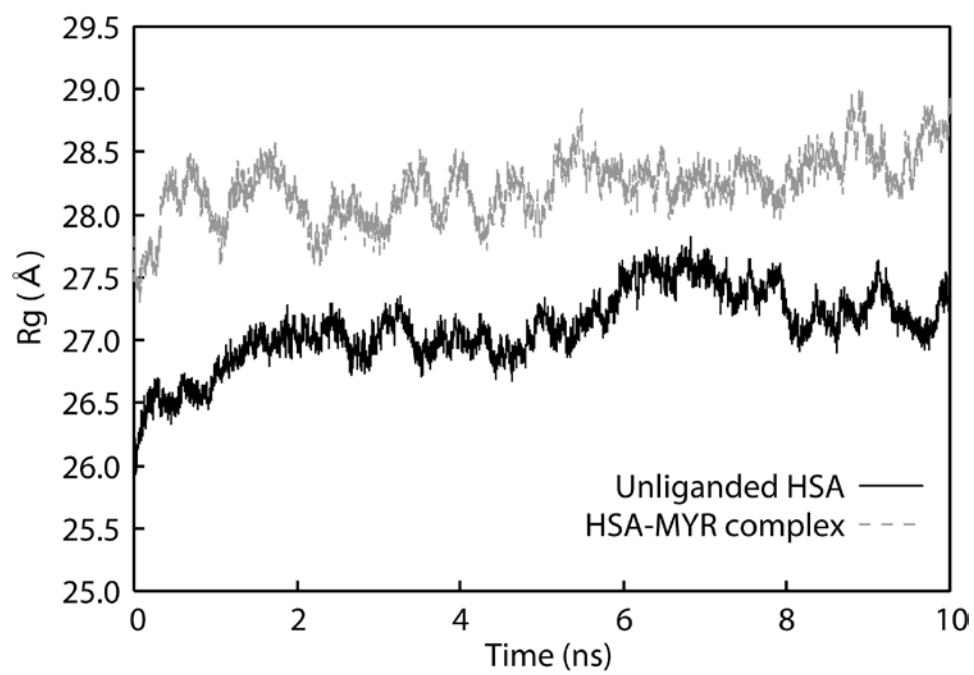


Fig. 4

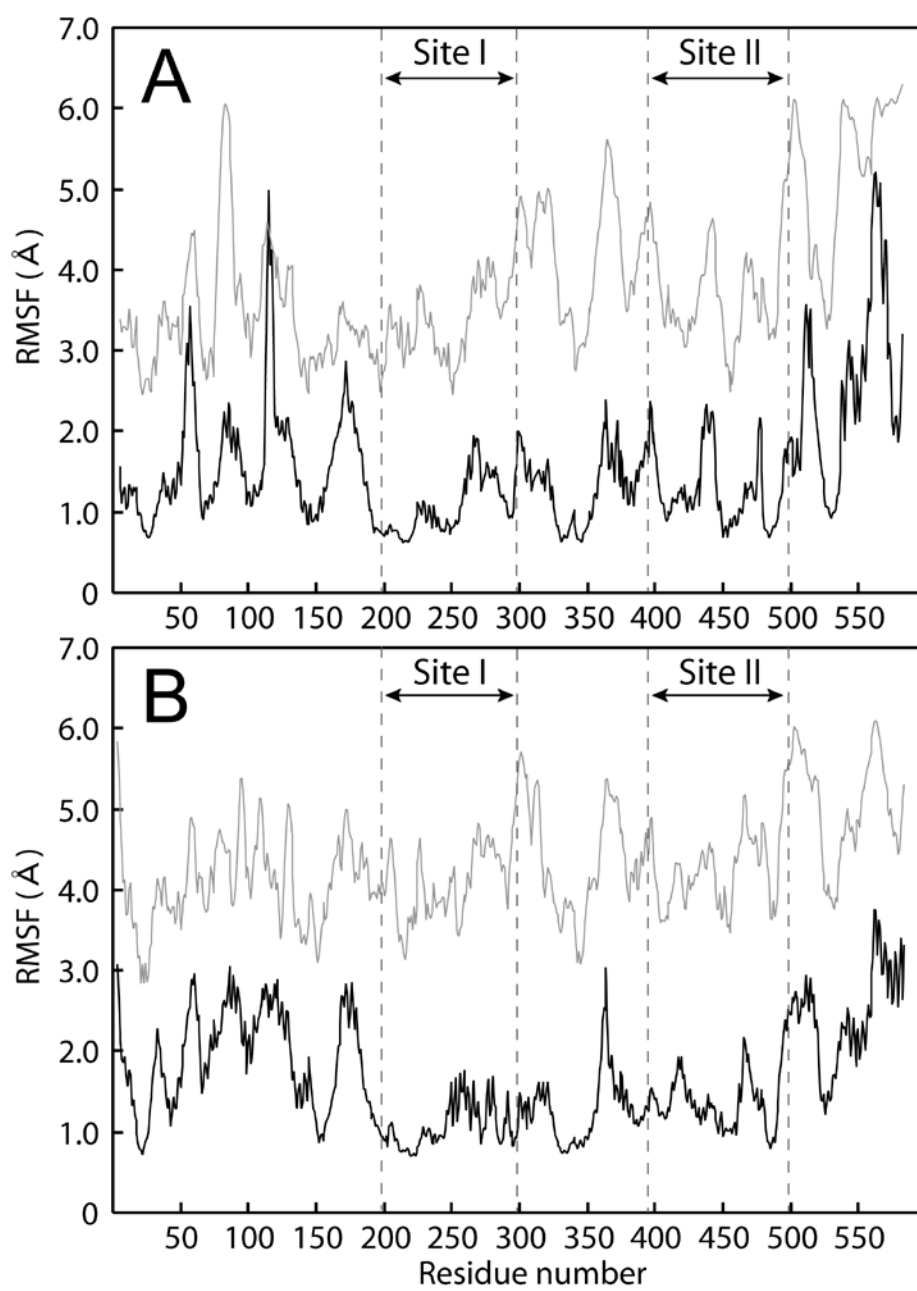


Fig. 5

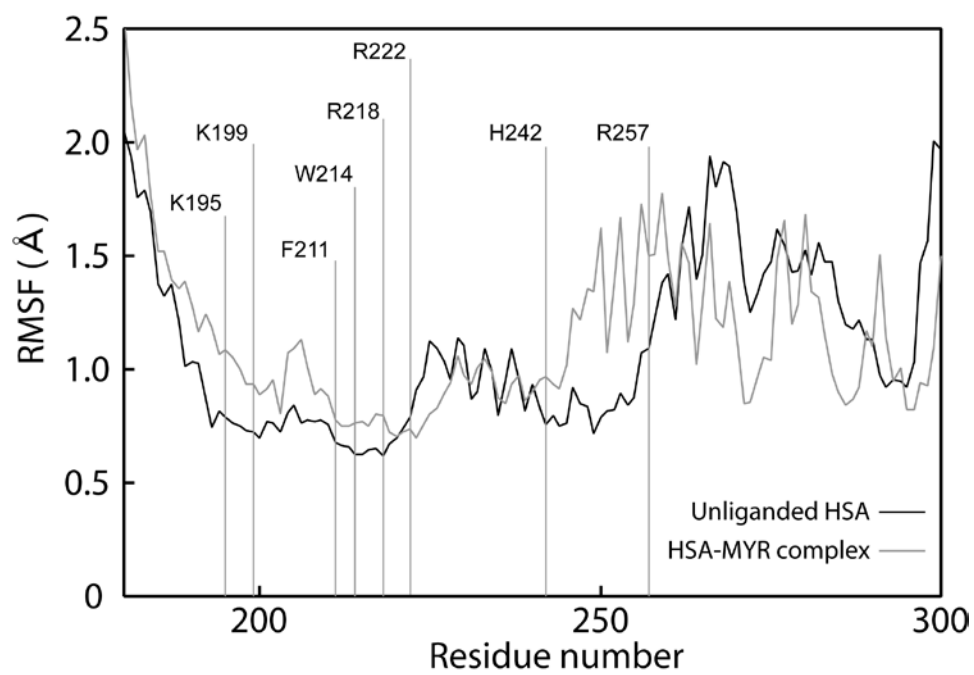


Fig. 6

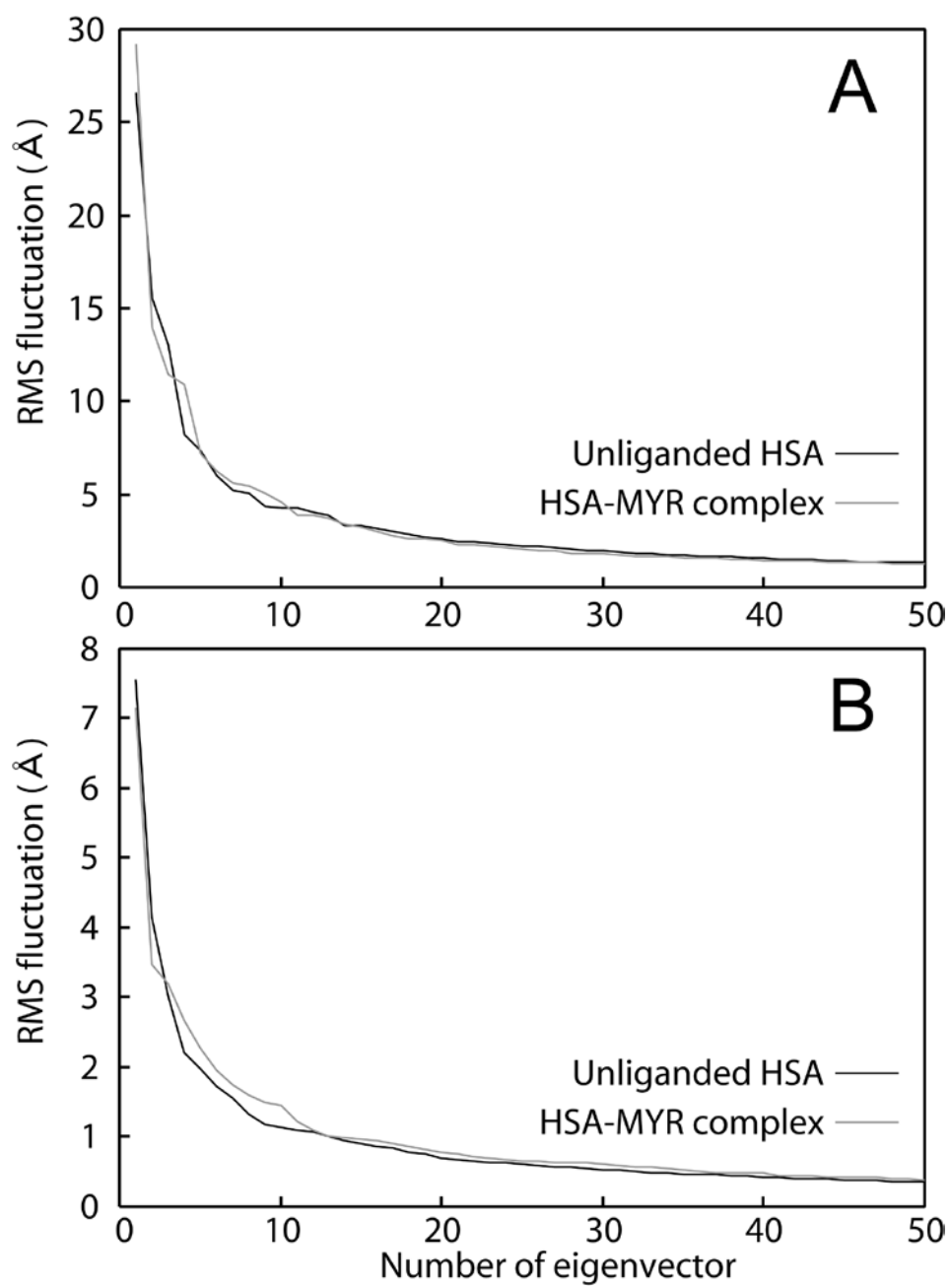


Fig. 7

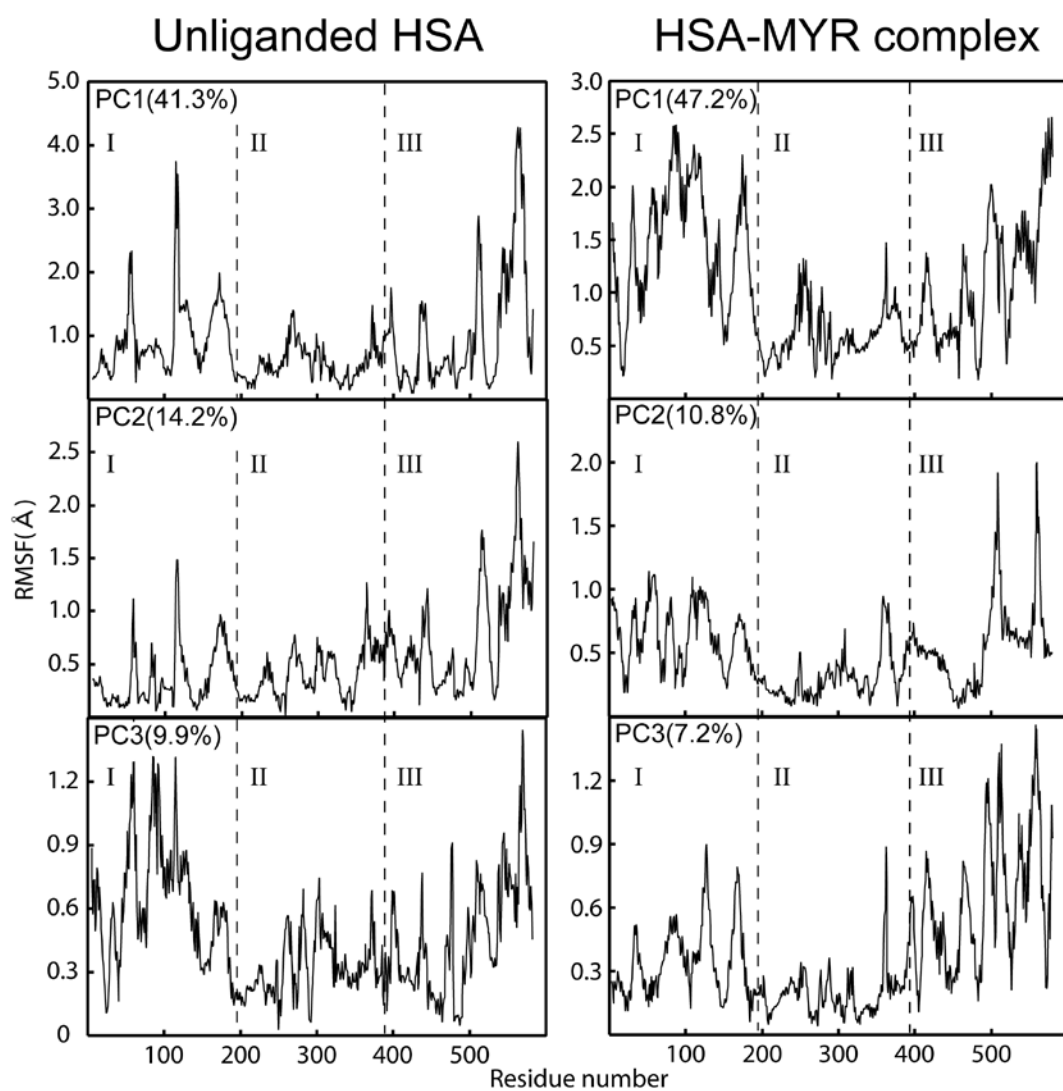


Fig. 8

